

Meta-Learning for Color-to-Infrared Cross-Modal Style Transfer

Evelyn A. Stump, Francesco Luzzi, *Member, IEEE* Leslie M. Collins, *Member, IEEE* Jordan M. Malof, *Member, IEEE*

Abstract—Recent object detection models for infrared (IR) imagery are based upon deep neural networks (DNNs) and require large amounts of labeled training imagery. However, publicly-available datasets that can be used for such training are limited in their size and diversity. To address this problem, we explore cross-modal style transfer (CMST) to leverage large and diverse color imagery datasets so that they can be used to train DNN-based IR image based object detectors. We evaluate six contemporary stylization methods on four publicly-available IR datasets – the first comparison of its kind - and find that CMST is highly effective for DNN-based detectors. Surprisingly, we find that existing data-driven methods are outperformed by a simple grayscale stylization (an average of the color channels). Our analysis reveals that existing data-driven methods are either too simplistic or introduce significant artifacts into the imagery. To overcome these limitations, we propose meta-learning style transfer (MLST), which learns a stylization by composing and tuning well-behaved analytic functions. We find that MLST leads to more complex stylizations without introducing significant image artifacts and achieves the best overall detector performance on our benchmark datasets.

Index Terms—automatic augmentation, convolutional neural network, cross modal, deep learning, infrared, transfer learning, meta learning, object detection, style transfer

I. INTRODUCTION

OBJECT detection is a computer vision task that has been dominated in recent years by deep neural networks (DNNs) [1]. DNNs are high-capacity non-linear models that require large quantities of annotated data to train effectively [1]. Therefore the success of DNNs can be partially attributed to the availability of large and public datasets, such as ImageNet [2] and COCO [3]. While such datasets are available for many color (RGB) imagery recognition problems, the datasets available for infrared (IR) imagery problems are far more limited. Several public IR datasets now exist (e.g., CAMEL [4], FLIR [5]), however, they are far more limited in size and diversity than color-based datasets, limiting the ability to effectively train or evaluate IR recognition models. There are many general strategies to mitigate this problem: more efficient use of data (e.g., data augmentation [6], self-supervised learning [7]), more effective modeling (e.g., ResNet [8], Transformers [9]), transfer learning [10], and more.

Another recently-studied strategy to overcome training data limitations is RGB-to-IR cross-modal style transfer (CMST) [11], which is the focus of this work. The goal of CMST

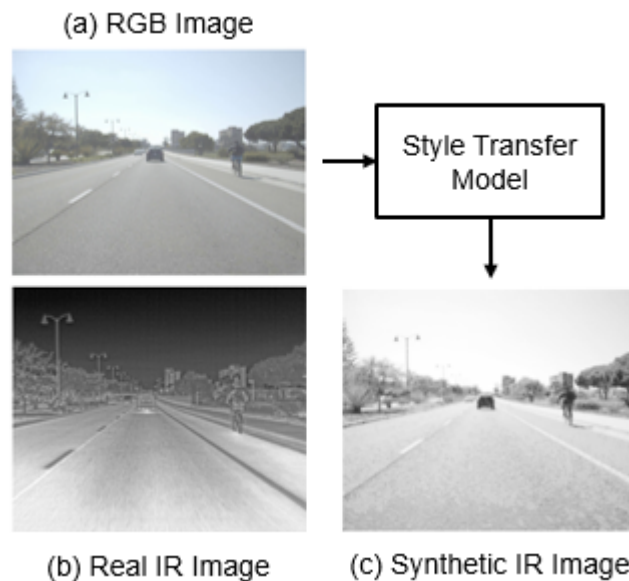


Fig. 1. An example of (a) an RGB image, (b) a real IR image and (c) a synthetic IR image produced by a style transfer model. Images from [5]

is to transform RGB (i.e., color) imagery so that it appears as though it were collected under similar conditions using an IR camera [11]. Fig. 1 illustrates CMST with a real-world pair of co-collected RGB and IR imagery. In this example, an ideal style transfer model will take the RGB image (Fig. 1(a)) as input and produce a synthetic IR image (Fig. 1(c)) that closely resembles the real-world IR image (Fig. 1(b)) that was co-collected with the RGB input image. If an accurate RGB-to-IR transformation can be found, it may be possible to directly leverage large existing RGB datasets (e.g., COCO, ImageNet) to train IR recognition models, alleviating the current bottleneck of IR training data.

Unfortunately however, deriving an accurate CMST model is challenging. The IR image of a scene depends upon many factors, such as the material composition and solar insolation of the scene content, as well as recent weather conditions in the scene (e.g., ambient temperature). Modeling the relationship between IR imagery and these underlying factors is challenging, even when full information about them is available. However, in CMST we must infer an IR image of some scene using only an RGB image of that scene. As a result, CMST models do not have (direct) access to many factors that influence the appearance of the IR imagery, and there are many valid IR images that could be paired with a given

J.M. Malof is with the Department of Electrical and Computer Engineering, Duke University, Durham, NC, 27705 USA e-mail: jmmalo03@gmail.com
Manuscript received April 19, 2005; revised September 17, 2014.

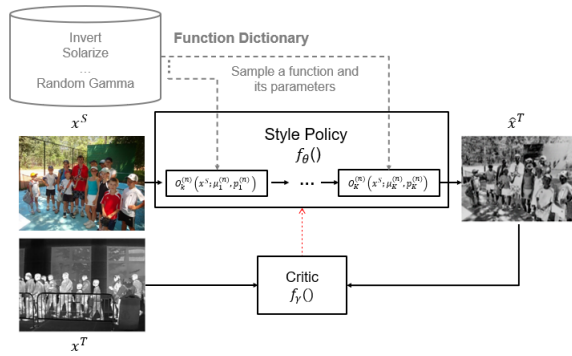


Fig. 2. This figure shows a diagram of our proposed MLST model. RGB imagery is stylized by a composition of k functions and function parameters (termed a ‘stylization policy’) sampled from a learned probability distribution. The loss of an adversarial critic (red line) is used as the training signal for the policy.

input RGB image. Here each plausible IR image corresponds to a different setting of the underlying scene conditions (e.g., temperature, insolation).

A. Existing Work on RGB-to-IR CMST

Despite the aforementioned challenges of RGB-to-IR CMST, recently-proposed CMST methods have shown promise [11]. One general CMST strategy has been to *hand-craft* models based upon known physics or heuristics relating RGB and IR imagery [12]. For example, the authors in [12] hand-crafted an effective CMST by composing several common image transformations (e.g., contrast enhancement, blurring). However, due to the complexity of the RGB-to-IR CMST, another approach has been to use machine learning (ML) to *infer* an effective model using data. In this case, an ML model learns a function that maps RGB into IR imagery using examples of imagery from each modality. *In principle*, ML models can leverage the increasingly large datasets of RGB and IR imagery to learn more complex and accurate CMST models than have been achieved with hand-crafted approaches. As a result, most recent CMST approaches are based upon ML, and in particular deep neural networks (see Sec. II for details).

Despite the variety of RGB-to-IR CMST methods, one limitation of existing work is that there is yet to be a comprehensive comparison of approaches. In particular, existing studies typically only compare their proposed methods against just one or two approaches. As a consequence, there are no studies exploring, for example, whether ML-based approaches outperform hand-crafted methods, or simple baseline approaches such as grayscale transformations. Existing work also only compares competing CMST methods on just one or two datasets. In recent years several new datasets have become available, making it possible to conduct more rigorous comparisons of RGB-to-IR CMST methods. Without a rigorous comparison of methods, it is difficult to determine the absolute and relative performance of existing RGB-to-IR CMST approaches, and the extent of methodological progress over time.

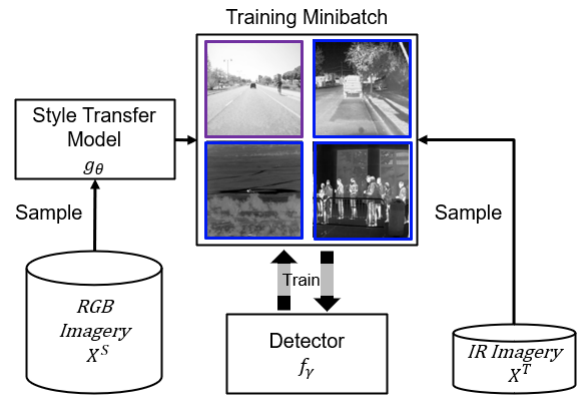


Fig. 3. An illustration of mixed batch training. RGB imagery is stylized by a style transfer model to create synthetic IR images. The synthetic IR imagery is used to supplement real IR data in training a detection model. A fixed proportion of each training minibatch is synthetic IR (purple outline) and the remaining images are real IR (blue outline).

B. Contributions of this Work

In this work we conduct a large-scale comparison of recent RGB-to-IR CMST models on four different publicly-available IR datasets. Our comparison includes several hand-crafted and data-driven CMST models, respectively, as well as simple baseline methods (e.g., identity and grayscale transformations). CMST can be seen as a special case of general style transfer, and we also include two successful ML-based style transfer methods: WCT2 [13] and CyCADA [14]. One key distinction between different ML-based approaches is whether they require paired or unpaired training data. In this work we focus upon studying *unpaired* CMST methods due to their wider applicability.

One challenge with benchmarking CMST models is performance evaluation. Recent publications have evaluated CMST models using manual visual inspection such as amazon mechanical turkers [12], [15], however, this makes it difficult to consistently and quantitatively compare methods. Another strategy has been to utilize paired RGB-IR datasets, and then evaluate the CMST model’s ability to predict the paired IR image given the input RGB image [16] [17]. This approach assumes the availability of *accurately* registered RGB-IR image pairs, which is a major limitation since few datasets satisfy this requirement. Another performance metric is to evaluate the effectiveness of the synthetic IR on some subsequent task that relies upon its photo-realism. In this work we evaluate the quality of CMST models using its synthetic IR imagery to train IR object detection models, as illustrated in Fig. 3. This criterion has been used in several recent CMST studies [18], [19], [16], [17], and was our major motivation for investigating CMST.

Based upon our benchmark experiments we find that existing ML-based CMST methods are outperformed by simple hand-crafted transformations. Our analysis suggests that this is because data-driven methods are either too simplistic, and therefore unrealistic or limited in variability; or they are too powerful, and often alter the semantic content of the scene. To overcome these limitations we propose meta learning

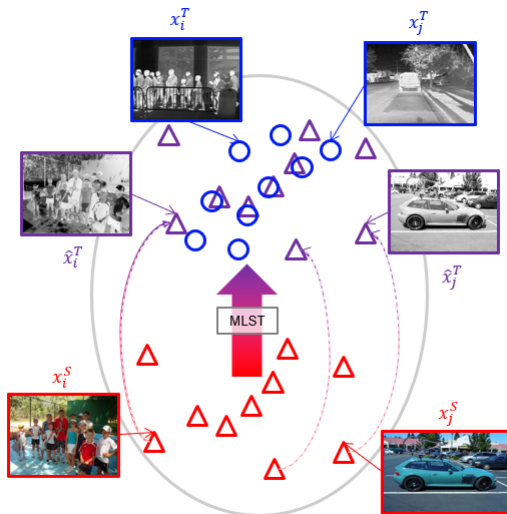


Fig. 4. A diagram of the training objective of MLST. RGB and IR images form clusters of imagery (red triangles and blue circles respectively) in feature space (gray ellipse). MLST uses the distance between these distributions as a training objective, the model learns a stylization policy that minimizes this distance in feature space between the real IR images and the new distribution of stylized RGB images (purple triangles) while maintaining good classification accuracy on the semantic objects.

style transfer (MLST), which models RGB-to-IR CMST as a composition of well-behaved analytic functions. This model is similar to successful existing hand-crafted CMST methods, but improves upon them by choosing the functions in the composition, and their parameters, using a data-driven method. A diagram of MLST along with real stylized RGB→IR imagery is shown in Fig. 2. We find that MLST learns more complex CMST models than hand-crafted models, but without altering the content of the underlying scene.

Our specific contributions can be summarized as follows:

- *The first comprehensive benchmark comparison of RGB-to-IR CMST models.* We present an objective comparison of several state-of-the-art stylization using performance on a downstream detection task as an evaluation metric across multiple benchmark datasets.
- *Meta-Learning Style Transfer (MLST), a state-of-the-art RGB-to-IR CMST model.* MLST offers superior performance on downstream detection tasks compared with existing state-of-the-art stylization methods. We also present an analysis of MLST showing that it is learning effective RGB-to-IR models, and closing the visual gap between RGB and IR imagery.

The organization of this paper is as follows: Section II discusses related work. In Section III we precisely define the CMST problem setting mathematically. Section IV presents MLST. In Section V we review the datasets used in this work. In Section VI we discuss the baseline CMST models we study in this work and review what datasets are used. In Section VII we present our experimental design and results; Section VII-A we perform additional experiments to analyze the primary benefits fo MLST. In Section IX conclusions about the work are drawn.

II. RELATED WORK

A. Image Style Transfer

RGB-to-IR CMST is a case of image style transfer(ST), which has been explored extensively in the context of texture mapping [11] [20] [21]. Modern ST methods rely primarily upon DNNs to align the distribution of the stylized imagery with real-world imagery in the target style. A seminal work is Gatys et. al. [22], where the authors hypothesized that the semantic content of an image is encoded in the activations (or features) of deep layers of a network, while the style (i.e., colors and textures) is encoded in the covariance of features in shallow layers of the network. In [22], content features and style features are extracted from two images I_c and I_s respectively. The output stylized image I is iteratively constructed by minimizing the weighted sum of a content loss objective and a style loss objective. The resulting image I has the semantic content from I_c while emulating the style of I_s .

Following the work of Gatys et. al., two general communities of ST emerged [11]. The first method we will discuss builds upon Gatys' approach directly and uses DNNs to isolate and align style and content from imagery. We refer to these methods as photorealistic style transfer (PST). The work in [23] proposed the whitening coloring transform (WCT) to address a weakness with Gatys' method: namely that each I_c and I_s pair requires a unique optimization. This does not scale well for stylizing a large number of images. To address this problem, [24] hypothesized that arbitrary stylization can be accomplished in two affine transformations: a 'whitening' transform that isolates the content features from I_c , followed by a 'coloring' transform that aligns the content and style features by maximizing covariance. However these transforms alone tend to erroneously produces artifacts in the stylized image, as a result of information loss inherent in the forward pass (specifically pooling layers) of DNNs [13]. The authors in [25], [15] address this limitation by adding a regularization objective/post-processing step to their models which takes advantage of known properties of photorealistic images (i.e., continuous edges) and use pooling masks to preserve spatial information that would otherwise be lost in the encoding process [15]. WCT2 [13] introduces a novel encoder with invertible pooling layers and uses multiple WCT transforms in their encoder for a more robust stylization. In this work, we use WCT2 as a representative example of PST models due to its state of the art performance compared to other PST models [13].

The second general class of ST methods is termed adversarial style transfer (AST). In these approaches some model (typically a DNN) - termed the critic or discriminator - is trained to distinguish stylized imagery from real imagery. Concurrently, the stylization model is trained to maximize the error of the critic. If the critic cannot distinguish between real and stylized imagery, then the stylization is assumed to be effective. The cycle-consistent generative adversarial network (CycleGAN) [26] is one widely-used AST model [11] [1]. However, a known problem with CycleGAN is that it can erroneously

TABLE I

THIS TABLE SHOWS THE FUNCTION DICTIONARY AVAILABLE TO MLST IN OUR EXPERIMENTS. THE LEFT COLUMN CONTAINS THE NAMES OF EACH FUNCTION. THE RIGHT CONTAINS THE DEFINITION OF EACH FUNCTION.

Function Name	Function/parameter Description
Random Brightness	Shift all pixels up/down by a random value $x \in U[-\mu, \mu]$
Random Contrast	Multiply all pixels by a random value $1 + x, x \in U[0, \mu]$
Solarize	Invert all pixels above pixel value μ
Random Gamma	Exponentiate all pixels values by a random value $x/100, x \in U[-\mu, \mu]$
Gaussian Blur	Gaussian Blur images with kernel with size $k = (3, 3)$ with standard deviation $\sigma = U[0, \mu]$
Invert	Invert Image
Identity	Do nothing

alter the semantic content of images [26], e.g. warp or remove objects in the imagery. CyCADA [14] addresses this limitation by adding a semantic consistency objectives to the model as well as a supervised task objective (e.g., classification, segmentation, detection, etc.). These losses encourage the preservation of semantic content in the stylized image. In this work, we use CyCADA as a representative example of AST models based on its state of the art performance. Additionally, we compare to CycleGAN as well as it is still widely used as a benchmark model in the style transfer community [11] [19] [27]. To our knowledge, CyCADA has not been used for RGB-to-IR CMST.

B. RGB-to-IR CMST

RGB-to-IR CMST can be conceived as a special case of ST where the goal is to create synthetic IR using RGB imagery as input. Some work in the CMST community uses AST methods directly such as [28], and [29] who applied adversarial auto-encoders and CycleGAN to RGB-to-IR CMST respectively. Other work builds upon more general ST models. In [19] the authors add a content-preserving connection structure to the generator of CycleGAN, and an ROI loss objective. Liu et. al. [19] add a supervised task loss to CycleGAN in the form of object level classification. The task loss incentivizes class conditional stylization, as objects of different classes/materials have different thermal characteristics and provides additional information during training [19]. The authors in [18] replace the adversarial objective with a distance and add a perceptual loss. Perceptual loss is a measure of similarity between images [?], used here as a content preserving objective [18]. However, neither [19] or [18] have made their code publicly available. The addition of content-preserving objectives and task losses to CycleGAN are conceptually similar to CyCADA. For this reason, we use CyCADA as a representative comparison to these models.

A subset of AST models assume the availability of paired RGB-IR imagery [11] [30]. Pix2Pix [30], [31], ThermalGAN [16], and InfraGAN [17] have been used for RGB-to-IR CMST. RGB and IR image pairs provides a direct mapping of pixel intensities from the RGB to the IR style, however paired imagery is not always available for IR detection problems. Although our proposed approach, MLST, does not require paired

imagery, we also compare to ThermalGAN and InfraGAN as state-of-the-art examples of paired ST models.

Another strategy has been to hand-craft transformations based upon physics or heuristics [12]. The authors in in ThermalDet [12] hand-crafted an effective CMST by composing several common image transformations (e.g., contrast enhancement, blurring) [32]. We include ThermalDet [12] in our benchmarking result as a strong hand-crafted baseline. Although not included in previous studies, we also include several simple hand-crafted transformations as baselines (e.g., identity, grayscale transforms).

As discussed in Section I-B, one limitation of existing work is that there is yet to be a comprehensive comparison of RGB-to-IR CMST approaches. Existing studies typically only compare their proposed methods against just one or two existing methods, and they do so on a limited number of datasets [12] [28] [33] [29]. In this work we compare to numerous methods, including existing state-of-the-art CMST methods, representative recent methods from the general ST community, and simple hand-crafted methods. We compare these methods on four public benchmark datasets - more than any previous study on this topic: FLIR [5], DSIAC [34], CAMEL [4], and Kaist [35]. These datasets have been previously employed for RBG-to-IR CMST [18], [19], [17] as well as IR object detection [36], [31], [37].

C. Meta Learning

Meta learning is a field of ML focused on optimizing the learning process itself [38]. Methods involving meta learning are diverse and applied in diverse problem settings such as Bayesian optimization [39], few-shot learning [40], adversarial defense [41], and reinforcement learning [42]. Meta learning optimization methods are often involved in non-differentiable problems settings such as ours [38]. A variety of meta learning techniques have been developed to make otherwise non differentiable problems amenable to gradient descent based optimization methods (i.e., backpropagation) [42], [43]. We adopt one such technique from the automatic augmentation community [44]. In [44], they develop a method to optimize a composition of functions and their parameters. We adopt their meta-learning method to optimize MLST.

III. PROBLEM SETTING

In this section we precisely define the problem of unpaired CMST, henceforth just referred to as CMST. In CMST, we

TABLE II
THIS TABLE SHOWS SUMMARY STATISTICS OF OUR DATASETS.

Dataset Properties	Benchmark Dataset				
	FLIR	DSIAC	CAMEL	KAIST	COCO
# Training Images	8.9E3	1.2E4	8.1E3	7.6E3	7.0E4
# Testing Images	1.3E3	6.5E3	2.6E3	2.3E3	N/A
# Mutual Classes	4	2	4	1	4
# Training Objects	6.7E4	2.5E4	3.1E4	1.9E4	3.1E5
Average Image Size (pixels)	512x640	512x640	256x336	512x640	478x512
Average Object Size (square pixels)	38	22	48	63	88
Source	[5]	[34]	[4]	[35]	[3]
Splits	Official	Random video CV	[4]	[18]	Official

assume that we have some collection of labeled RGB imagery, $(X^S, Y^S) = \{(x_i^S, y_i^S)\}_{i=1}^{N^S}$, termed the *source data*, where $y^S \in \mathcal{Y}$ may take different forms depending upon the recognition task of interest (e.g., segmentation, object detect, and classification). We assume that $x_i^S \sim d^S$, where d^S is termed the source domain distribution. We also assume the availability of some IR imagery of the form $(X^T, Y^T) = \{(x_i^T, y_i^T)\}_{i=1}^{N^T}$ where the labels are similar to those in the source domain, so that $y^T \in \mathcal{Y}$. Here we assume $x_i^T \sim d^T$ and that $d^T \neq d^S$. Our goal is to train a generative model of the form $y = f_\theta(x)$ using both the source and target domain datasets. We assume there exists some function $\hat{x}^T = g(x^S)$ such that $\hat{x}^T \sim d^T$. Our goal is to infer a model, $\hat{g}_\theta(\cdot)$ that approximates the true underlying function $g(\cdot)$, where θ refers to potential parameters of our model.

Performance Evaluation. Evaluating the quality of a stylization model (e.g., compared to other competing models) is challenging because paired imagery is not always available. Furthermore, even where paired imagery is available, the stylization function g can be non-unique in general (see Sec. I), so that any specific IR image pair represents just one of many valid stylizations. Therefore a model cannot necessarily be penalized if its stylization does not match a particular IR pair. To overcome this obstacle we propose to evaluate CMST models based on the effectiveness of its imagery when training a task model of the form $y^T = f_\gamma(x^T)$. We propose a specific evaluation criterion in Sec. VII-A.

Important CMST sub-problems Existing CMST models are often designed with specific assumptions about the data that is available for training \hat{g}_θ , resulting in several specific sub-problems of CMST. One potential assumption regards the availability of task-specific labels in the source and/or target domains (i.e., Y^S and Y^T). If such labels are assumed available, then we refer to this as *supervised* CMST, and *unsupervised* CMST otherwise. Another important assumption regards the relationship between X^T and X^S . If the data is paired, so that each $x^T \in X^T$ has a corresponding image $x^S \in X^S$ that was collected under similar conditions (e.g., capturing the same scene content, at the same time) then the problem is said to be *paired* CMST, and *unpaired* otherwise.

IV. META LEARNING STYLE TRANSFER

In this section we describe our proposed approach, termed Meta Learning Style Transfer (MLST), which models RGB-to-IR CMST as a composition of several functions (e.g., contrast changes, blur) as illustrated in Fig. 2. In our benchmark experiments described in Sec. VII we found that CMST models comprising a composition of relatively simple functions often outperformed more expressive DNN-based approaches (e.g., WCT2, CycleGAN). We hypothesized that these compositional methods might achieve much greater performance if they could be designed and optimized using data-driven methods, rather than via manual trial-and-error; this is the fundamental motivation for MLST.

Model Description. In MLST we assume the availability of a set, or "dictionary", of N candidate functions, where $O^{(n)}(\cdot)$ represents the n th function in the dictionary. Each function has associated with it a probability of being applied to an image $w^{(n)}$, a parameter (i.e., a magnitude or a threshold) $\mu^{(n)}$, and a logical flag $p^{(n)}$. Each function is represented by a Bernoulli random variable of the form

$$x \leftarrow \begin{matrix} O^n(x; \mu^{(n)}) & p = p^{(n)} \\ x & p = 1 - p^{(n)} \end{matrix} \quad (1)$$

In principle the user can include any function whose input and output are both images, however, in our implementation we will try to choose functions that are likely to contribute towards a realistic stylization. We only require that each function only have one $\mu^{(n)}$ parameter associated with it. The dictionary of functions used is provided in Table I.

A composition of k functions termed 'stylization policy' are applied in sequence, where $k \in [1, 2, \dots, K]$ as shown in Fig. 2. $O_k^{(n)}(\cdot)$ represents the n th function in the k th step in the policy. What function is applied at each step is sampled from a categorical distribution. The final output of MLST is shown in Alg. 1 where w represents a vector of weights, σ the softmax function, and \mathcal{C} the categorical distribution.

Model Parameter Optimization. The goal of MLST is to estimate the parameters w_k and μ_n^k . We aim to develop a method that could utilize data to infer both (i) the functions that should be included in the composition, (ii) the order in which they should be applied, and (iii) any parameters

Algorithm 1 MLST Stylization

```

x: input image
 $w_k, \mu_k^{(n)}$ : learned parameters
 $\sigma$ : softmax function
 $\mathcal{C}$ : categorical distribution
while  $k$  in 1, ...  $K$  do
   $(n) \sim \mathcal{C}[\sigma(w_k)]$ 
   $x \leftarrow O_K^{(n)}(x; \mu_k^{(n)}, p_k^{(n)})$ 
   $k++$ 
end while
return x

```

μ associated with each function. Direct optimization of this objective is computationally intensive because, in general, the functions are represented through stochastic nodes which makes them not amenable to backpropagation. Additionally each function may be highly non-linear and also may not be analytically differentiable. During training, we approximate the output of the k th layer of the stylization model $f_\theta()$ as

$$x \leftarrow \sum_{n=1}^N \sigma(p_k^n) O_k^n(x; \mu_k^{(n)}, p_k^{(n)}) \quad (2)$$

where σ is the softmax function. The output of the model is shown in Alg. 2. To find the ideal stylization policy, we differentiate each operation with respect to p and μ .

Algorithm 2 MLST Search

```

x: input image
 $w_k, \mu_k^{(n)}$ : learnable parameters
 $\sigma$ : softmax function
 $\mathcal{C}$ : categorical distribution
while  $k$  in 1, ...  $K$  do
   $x \leftarrow \sum_{n=1}^N \mathcal{C}[\sigma(w_k)]^{(n)} O_K^{(n)}(x; \mu_k^{(n)}, p_k^{(n)})$ 
   $k++$ 
end while
return x

```

Recent results in the meta learning [38] and automatic augmentation communities [44], [45] [46] propose and evaluate mathematical methods to optimize these otherwise non-differentiable functions via backpropagation, making it substantially more computationally efficient. In this work, we use the meta learning based optimization established in [44]. In [44] this loss was used to perform augmentation, in which the goal of the model was to learn an ideal way to augment RGB imagery, rather than perform CMST. Therefore, the goal was to alter the imagery while still ensuring that the stylized imagery looked like real RGB imagery. This is a different, and potentially simpler, operation than mapping from one modality to another. It is therefore unclear whether such an adversarial method is sufficient for learning an effective CMST mapping.

Using gradient descent based methods (i.e., backpropagation [47]) to learn these parameters presents a challenge. Each node of the stylization model f_θ represents a stochastic quantity.

Random nodes are not amenable to backpropagation, as we cannot evaluate error gradients with respect to a random variable [48]. In [48], the authors propose the reparameterization trick for backpropagating through nodes that represent Gaussian random variables for variational autoencoders (VAEs). The reparameterization trick approximates the random variable as fixed with the 'source' of the randomness being controlled by a dummy random variable. An equivalent of the reparameterization trick for binomial distributions was proposed in [49] and adopted in [44] which we base our method upon. Instead of a Bernoulli distribution, each operation is modeled by the relaxed Bernoulli distribution. It is of the form

$$ReBern(b; p, \lambda) = \zeta\left(\frac{1}{\lambda} \left[\log \frac{p}{1-p} + \log \frac{u}{1-u} \right]\right) \quad (3)$$

where ζ is the sigmoid function that keeps the function in the range $[0, 1]$, and $u \in U[0, 1]$, $b \in Bern[0, 1]$ and λ is the 'temperature' of the sigmoid function, low λ causes $ReBern(b; p, \lambda)$ to behave like a one-hot vector. In this representation, the randomness is controlled by the dummy variable u . With this approximation $O(x; \mu, p)$ is differentiable with respect to p .

Some functions have discrete values of μ^n (e.g., solarize) or do not have continuous derivatives. In such cases, we use the straight through approximation [44] to estimate the gradient as

$$\frac{\partial O(x)}{\partial \mu} \approx 1 \quad (4)$$

With this approximation $O(x; \mu, p)$ is differentiable with respect to μ .

For a critic, we used a ResNet-18 [50] and replaced the classification layers with a two-layer network. A similar critic is used in [44] [42]. A classification 'task' loss is added to prevent images of a specific class from being stylized into images of another class. This approach was chosen to preserve the different spectral statistics associated with different materials which correspond to each class. For instance, people are usually bright in IR imagery but a car with the engine off is not bright. The training of our algorithm is shown in Alg. 3

V. EXPERIMENTAL DATASETS AND HANDLING

In this section we discuss the major datasets used in our experiments, any modifications that we made to them, and (where applicable) the way we partitioned them into training and testing subsets to support our benchmark experiments described in Section VII. Table II summarizes the major details for each dataset.

A. Benchmark Infrared Datasets

FLIR¹ [5] This is a collection of street view RGB and mid wave IR (MWIR) imagery. Data is collected from multiple streets during the day and the night. The data is partitioned into training and testing sets by the developers [5], and we

¹<https://www.flir.com/oem/adas/adas-dataset-form/>

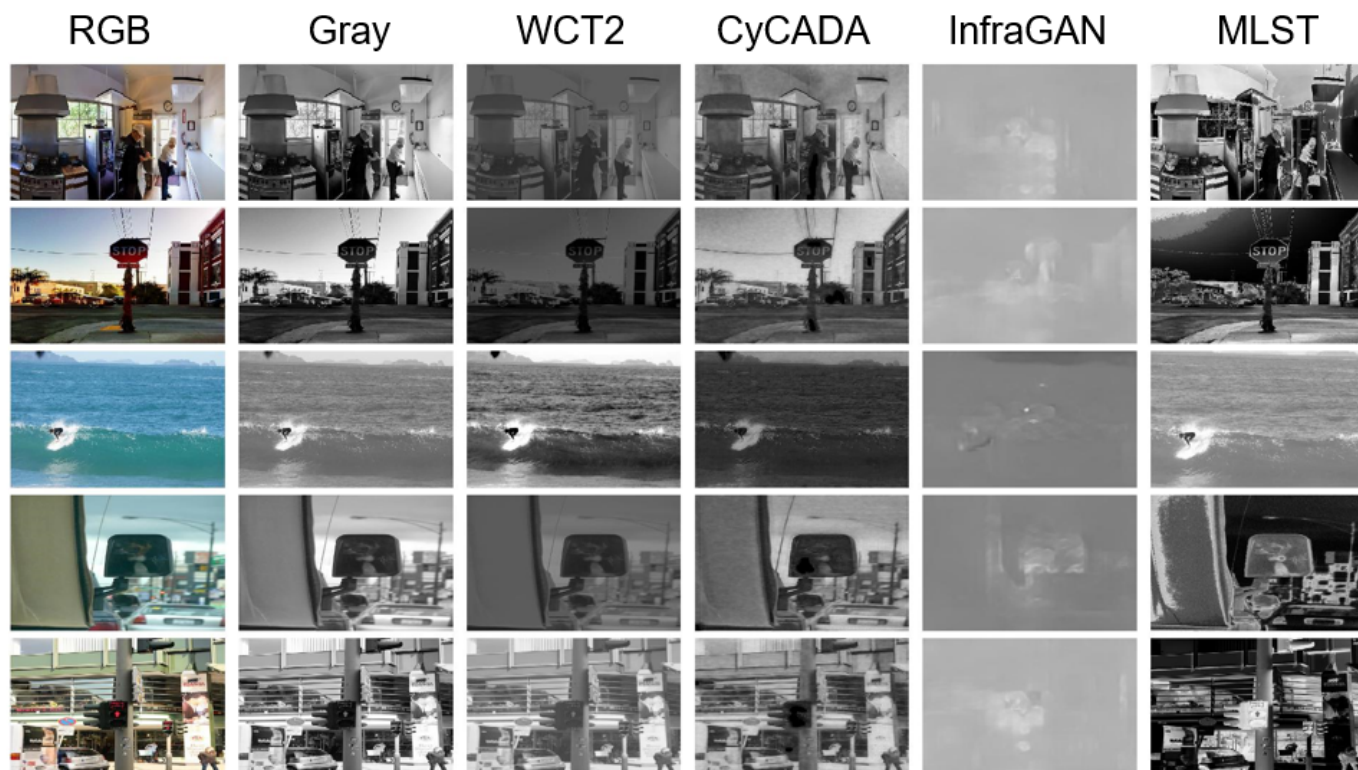


Fig. 5. Example imagery produced by each CMST method we evaluated. Each column of the matrix is five representative images all stylized by an NST algorithm. Gray and WCT2 are both very similar, CyCADA introduces artifacts into the imagery, and InfraGAN saturates images when deployed on out-of-domain images. MLST introduces no artifacts and produces a relatively complex nonlinear stylization.

TABLE III
THIS TABLE SHOWS THE OUR EXPERIMENTAL RESULTS, THE WINNER IN EACH DATASET IS BOLDDED.

Method	Paired?	Supervised?	Benchmark Dataset Performance (mAP@0.5)				AVG
			FLIR	DSIAC	CAMEL	KAIST	
None (Baseline)	N/A	N/A	.647	.593	.582	.427	.562
Identity	N/A	N/A	.650	.660	.610	.478	.599
Grayscale (Inversion)	N/A	N/A	.676	.660	.684	.488	.627
Grayscale	N/A	N/A	.666	.640	.693	.478	.619
ThermalDet [12]	N/A	N/A	.628	.689	.641	.485	.612
WCT2 [13]	N	N	.642	.660	.643	.490	.609
CycleGAN [26]	N	N	.600	.669	.603	.451	.581
CyCADA [14]	N	N	.640	.684	.634	.469	.608
CyCADA [14]	N	Y	.647	.686	.666	.469	.617
MLST (Ours)	N	N	.629	.716	.749	.459	.638
MLST (Ours)	N	Y	.653	.723	.751	.471	.650
ThermalGAN [16]	Y	Y	.642	.675	.615	.475	.601
InfraGAN [17]	Y	N	.666	.687	.653	.479	.621

Algorithm 3 MLST Train

f_θ : stylization model
 f_γ : task (classification) model
 $d_\theta(\cdot, \cdot)$: distance between two densities with learnable parameters θ
 $\mathcal{L}, \mathcal{L}_\gamma$: cross-entropy loss, task loss
 ϵ task loss coefficient
 $\{X^T, Y^T\}, \{X^S, Y^S\}$: training distributions
while not converge **do**
 Sample a pair of batches B^T, B^S from X^S, X^T
 Stylize data $\hat{x}^T = f_\theta(x); (x \in B^S)$
 Measure distance $d = d_\theta(B^T, \hat{B}^T)$
 Compute task loss $\mathcal{L}_\gamma = \sum_{B^S} f_\gamma(\hat{x}^T, \hat{y}^T) + \sum_{B^T} f_\gamma(x^T, y^T)$
 $\arg \min_{\theta} (d + \epsilon \mathcal{L})$
end while

adopted this handling for our experiments. It has been widely used in both the IR object detection communities [51] [52] and the CMST communities [17].

DSIAC² [34] This dataset is a collection of MWIR imagery. Objects of each class are represented at several ranges for both day and night. Targets moved at a constant velocity in a circular pattern at each range, allowing the targets to be consistently imaged at the same locations and all aspect angles. We only include imagery that contains the people and civilian vehicles (e.g., trucks, SUVs, etc.) because these classes are represented in our RGB source data: MS COCO [3]. Objects in this dataset appear at ranges 500-5000m from the camera. Objects in COCO (and the other IR datasets) appear much closer to the camera. For this reason, we only include videos where targets appear at (approximate) distances of 500-3500m from the camera such that objects in DSIAC appear similarly to the same objects in COCO while still retaining a large volume of data. We used random video-based cross validation to create a training dataset and testing dataset which comprise 80% and 20% of all videos, respectively. Lastly, we extract every 10th frame from all videos to minimize visual redundancy in the dataset. It has been used for IR object detection [53] [54], and for CMST [12] [19].

CAMEL, [Gebhardt et al., 2019] [4] This data is a collection of IR data representing road scenes and pedestrian scenes. Data is collected from fixed cameras viewing different locations representing indoor and outdoor scenes with some locations filmed during the day and others at night. We used a video-based training and testing partition suggested by the authors. CAMEL has been used in IR object detection [55], but to our knowledge has not been evaluated in the context of CMST. We use the train and test partitions proposed by [4].

KAIST, [Choi et al., 2019] [35] This dataset is a collection of street view RGB and MWIR imagery. Data was collected across multiple locations during both the day and night. We used the same train and test partitions used in [18]. Kaist has been widely used in both the IR object detection communities [51] [56] and the CMST communities [29] [18] [17].

ThermalWorld, [Kniaz et al., 2018] [16] is a collection of RGB and MWIR street view imagery. Crucially, this dataset has segmentation labels available. We use all the training imagery in ThermalWorld for training ThermalGAN VI, but do not use it in evaluation. The dataset is unsupported, and a fraction of the data files published by the author are unavailable. As such, as far as we know, it has not been widely used in either the object detection or CMST communities.

B. Source RGB Imagery: COCO

COCO is a large dataset of RGB images [3]. It consists of thousands of RGB images labeled with ground truth annotations and represents 80 classes. From among the training data, we only use COCO images which contain a class of object that is represented in the IR data and only labels which correspond to those objects: people, bikes, cars, and dogs (COCO classes 1, 2, 3, and 18 respectively).

VI. EXISTING STYLIZATION MODELS

In this section we briefly describe the existing stylization models that were used as baseline stylization methods in our benchmark experiments. Due to space limitations, we summarize the following major features of each model, and refer the reader to references for further details: (i) seminal publication(s) on the method, (ii) why we included it in our study, and (iii) a brief description of how it works, including loss functions, where applicable. For precise implementation details of each model we refer the reader to our supplemental materials. Any model parameters that were not specified by these publications were optimized by finding a local maximum on our downstream detection task using a greedy forward sequential search.

Gray, and **Gray-Inv.** are included as a naive, non data driven stylizations. We average the color channels of all COCO images. For Gray-Inv we also invert the pixel intensities of every COCO image (0 becomes 255 and vice versa).

ThermalDet [12] is included as a non data-driven model that is more complex than a naive grayscale stylization. It is a composition of image transforms (e.g., contrast enhancement, brightness shift, etc.). We preprocess all COCO images using the methods and parameters proposed in [12].

WCT2 [13] is used as a representative example of PNST models for this study. We use the official implementation described in [13]. The WCT transform itself has a closed form solution. WCT2 requires image pairs for stylization. Each RGB image is paired with a random IR image; because COCO is larger than all IR benchmarks combined some IR images are used to stylize multiple COCO images.

CycleGAN [26] is still a widely used model for ST tasks and is frequently used as a benchmark model in several ST papers [1], [11], [17]. We included it in this work as a representative example of AST models. We used the official implementation described in [26]. The model has two discriminator and generator pairs. The training signal of a generator depends on two arguments: a discriminator (classification) loss

²<https://dsiac.org/technical-inquiries/notable/infrared-imagery-datasets/>

TABLE IV
THIS TABLE SHOWS THE OUR EXPERIMENTAL RESULTS, THE WINNER IN EACH DATASET IS BOLDED.

Method	Uses COCO?	Benchmark Dataset Performance (mAP@0.5)				AVG
		FLIR	DSIAC	CAMEL	KAIST	
None (Baseline)	N	.647	.593	.582	.427	.562
Grayscale (Inversion)	Y	.676	.660	.684	.488	.627
Aug	N	.632	.657	.641	.419	.587
MLST Aug	Y	.646	.664	.610	.454	.594
MLST Style	Y	.653	.723	.751	.471	.650
MLST Style + MLST Aug	Y	.662	.713	.769	.481	.654

$L_{gan}(\cdot)$ and a cycle consistency loss $L_{cyc}(\cdot)$. The loss function is of the form

$$\mathcal{L} = L_{gan}(D_T(\hat{x}^T)) + L_{cyc}(\|g_{T \rightarrow S}(g_{S \rightarrow T}(x^S) - x^S)\|_1) \quad (5)$$

where $D_T(\cdot)$ represents the discriminator model for domain T , $g_{S \rightarrow T}$ represents the generator that stylizes images from domain S to domain T and $g_{T \rightarrow S}$ represents the generator that stylizes images in the opposite direction. For simplicity, the loss of the second generator is excluded. We trained our model using all training images from all IR benchmarks and all training images from COCO.

CyCADA [14] is used as a representative example of state-of-the-art adversarial style transfer models in this work. We use the official implementation described in [14]. CyCADA has a loss function similar to CycleGAN, but with two additional terms: a task loss $L_{task}(\cdot)$ which adds supervised information to training and a semantic consistency loss $L_{sem}(\cdot)$ which helps to preserve content in the stylized image. The loss of the generator is of the form

$$\mathcal{L} = L_{gan}(D_T(\hat{x}^T)) + L_{cyc}(\|g_{T \rightarrow S}(g_{S \rightarrow T}(x^S) - x^S)\|_1) + L_{task}(f_\gamma(\hat{x}^T), \hat{y}^T) + L_{sem}(L_{task}(f_\gamma(\hat{x}^T), \arg \max(f_\gamma(\hat{x}^S)))) \quad (6)$$

where the semantic consistency loss is defined by predicting the labels from a fixed classifier. This encourages the stylized image to be classified the same way in both domains. For simplicity, the loss of the second generator is excluded. We trained our model using all training images from all IR benchmarks and all training images from COCO.

ThermalGAN [16] is used as a representative example of paired CMST models. We used the official implementation discussed in [16]. Stylization is achieved in two stages. The first stage tries to predict coarse temperature maps from RGB images which are proportional to average temperature maps based on segmentation labels $X^{T'}$. The second stage predicts fine texture variation within the coarse thermal map. This model uses an L1 loss at each stage along with an adversarial discriminator as training signals to train both generators. The loss function is of the form

$$\mathcal{L} = L_{gan}(D_T(\hat{x}^T)) + \|(g_{S \rightarrow T'}(x^S) - x^{T'})\|_1 + \|(g_{T' \rightarrow T}(x^{T'}) - x^T)\|_1 \quad (7)$$

where $x^{T'}$ represents the coarse thermal image, $g_{S \rightarrow T'}$ is the generator that predicts $x^{T'}$ and $g_{T' \rightarrow T}$ is the generator which adds fine texture detail to $x^{T'}$. We train and evaluate the model on the ThermalWorld dataset.

InfraGAN is used as a representative example of state-of-the-art paired CMST models. We used the official implementation in [17]. The model uses an L1 and SSIM objectives in addition to an adversarial discriminator as training signals for the generator. The loss function of the generator is of the form

$$\mathcal{L} = L_{gan}(D_T(\hat{x}^T)) + L_{cyc}(\|(g_{S \rightarrow T}(x^S) - x^T)\|_1) + L_{ssim}(SSIM(\hat{x}^T, x^T)) \quad (8)$$

where $SSIM(x, y)$ is the structural similarity metric [17], measuring similarity between two images.

VII. EXPERIMENTS

A. Experimental design

In our experiments, we systematically create stylized versions of COCO using each CMST method described in Sec. VI. Aside from exceptions noted below, each benchmark CMST model was trained on the same training dataset of unpaired IR and RGB imagery. The IR portion of the dataset comprised all of the imagery from the four benchmark IR datasets described in Sec. V. The RGB portion of the dataset comprised all imagery in our downsampled MS COCO dataset described in Sec. V. Models were trained to convergence on this training dataset (shared by all models), which was achieved in about 40 epochs in each case. We then optimized hyperparameters of each model using a greedy forward sequential search based on the performance of a task model. Additional details about the training process of each model can be found in the supplemental materials.

Due to limitations associated with ThermalGAN, and InfraGAN these models were trained differently from the other

models. ThermalGAN requires paired IR-*RGB* data and thermal segmentation labels during training. This information is not available on any of our four benchmark datasets, and therefore we trained ThermalGAN on the ThermalWorld dataset, which was the same dataset used to train ThermalGAN in the paper where it was introduced [16]. The single resulting ThermalGAN model was then deployed for stylization on all four of our benchmark tasks. InfraGAN also requires *RGB-IR* image pairs. Of our four benchmarks, three have *RGB-IR* image pairs (FLIR, CAMEL, Kaist). We trained InfraGAN on these three datasets in aggregate and then used the resulting model for stylization for all four benchmark tasks.

We then use the stylized data and real *IR* data to train a task model, f_γ , on each benchmark dataset. To regularize the effect of using stylized data in fine tuning, we construct each minibatch as a mix of stylized and real *IR* images, specifically 1 stylized *RGB* image in an 8 image training batch. A diagram of our experimental design is shown in Fig. 3.

Task Model and Performance Metric We use a YoloV3 object detection model (YOLO) as our task model. The implementation of the model is described in [57]. This implementation was chosen because it was a python implementation of YOLO and publicly licensed. To measure the performance of our models, it is common to use the Intersection Over Union (IoU) score to classify each prediction as correct, a false alarm, or a miss. We then measure the Precision and Recall scores of each detector [58]. By the conventions of each dataset, we report mean average precision at an IoU of 0.5, or mAP@0.5 (mAP) score [5], [35]. A higher mAP score is indicative of a more realistic stylization.

B. Experimental results

The quantitative results of our experiments are shown in Table III. The results indicate that using CMST is always beneficial (i.e., higher mAP score) compared to using no CMST (i.e., the *None (Baseline)* method). Surprisingly, even using the *Identity* stylization - equivalent to supplementing with raw *RGB* imagery - is still highly beneficial. Furthermore, this approach is consistently beneficial; on all four benchmark datasets it improves over the *None* method. We hypothesize that the diversity of content in the MS COCO dataset outweighs the disadvantages of training directly upon *RGB* imagery, which is a different modality and therefore known to be visually distinct compared to *IR* a priori.

The *Identity* method also represents an important baseline for any other more sophisticated CMST methods; if they are effectively stylizing the *RGB* imagery then we would expect that these methods should be even more advantageous than the *Identity* model. The results indicate that simple grayscale transformations - represented by *Grayscale (Inversion)* and *Grayscale* - do indeed improve over the naive *Identity* method. These results suggest that, despite their simplicity, these methods do *tend* make *RGB* imagery more visually similar to *IR*. Notably, the *Grayscale(Inversion)* is never harmful compared to *Identity*, and improves over it in three out of our four benchmark datasets.

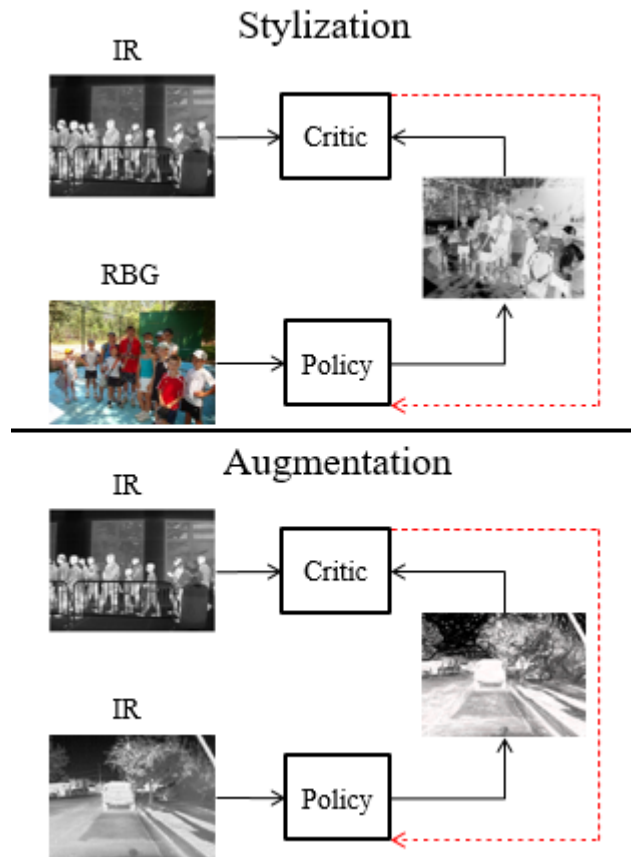


Fig. 6. This figure shows how MLST is trained for stylization (top) and how MLST is trained for augmentation (bottom). For stylization only *RGB* imagery is acted upon by the policy during training. For augmentation *IR* imagery is acted upon by the policy in training.

Surprisingly, nearly all of the data-driven CMST models perform more poorly (i.e., lower mAP) than the simple *Grayscale (Inversion)* method. There are only two exceptions to this: the unsupervised and supervised *MLST* models. The precise causes for inferior performance among the other data-driven models is unclear, however, some insight can be drawn by inspection of their stylized imagery. Example stylized imagery produced by several of the data driven models is shown in Fig. 5. Based upon this imagery, it appears that the data-driven models sometimes create artifacts in the stylized imagery, and reduce the dynamic range of the pixel intensities. By contrast, and by design, *MLST* introduces few or no artifacts into the imagery, and seems to maintain or expand the dynamic range of the stylized imagery.

The best-performing CMST models on average are the unsupervised *MLST* model and the supervised *MLST* model respectively. As expected the supervised *MLST* model achieves somewhat better performance, owing to the use of additional information during training (i.e., downstream task labels). We also observe that supervision improved the CyCADA model, although it achieved lower overall performance. The unsupervised and supervised *MLST* models improve over the *Baseline* method by 13.5% and 15.7% respectively. Importantly, they also improve over the simple *Grayscale (Inversion)* method,

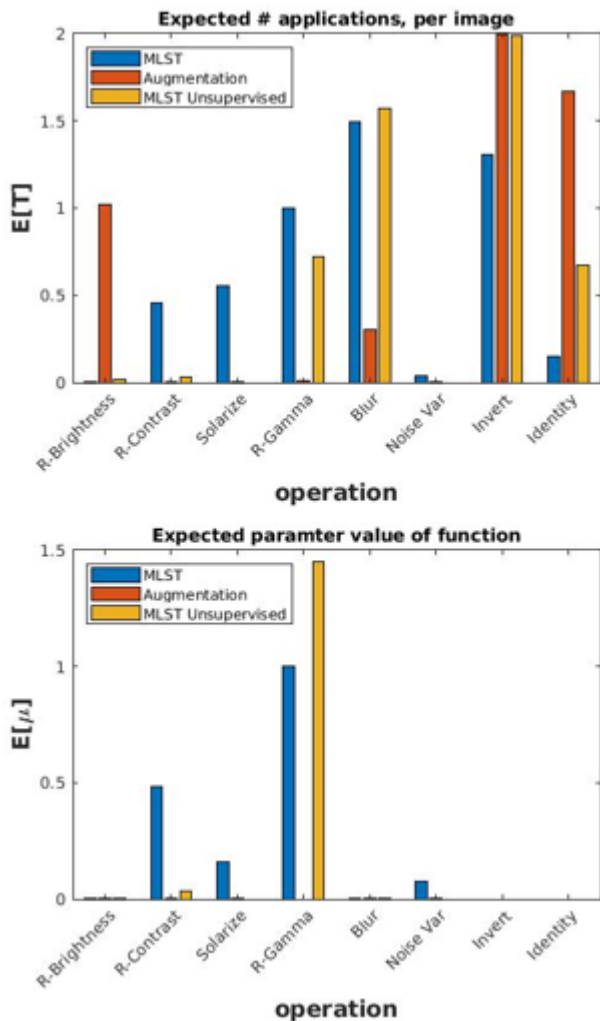


Fig. 7. This figure shows the differences in learned policies of MLST when used for stylization (blue), augmentation (orange), and unsupervised MLST (yellow). The top plot shows the expected number of times each operation in the dictionary is applied to an image $E[T^{(n)}]$. The lower plot shows the average parameter value of each operation $E[\mu^{(n)}]$. Note that operations invert and identity have no parameter and their $E[\mu^{(n)}]$ is set to zero.

on average, and are the only two data-driven methods to do so. Although supervised MLST does not always achieve the best performance on every individual dataset, it achieves the best performance compared to all other models on two of the four benchmark datasets.

VIII. ANALYSIS

In this section we conduct further analysis to characterize MLST. We observe that MLST is beneficial, but want to consider whether the effects are due to the statistical alignment of RGB imagery with IR, or because we are essentially augmenting the imagery? Or alternatively, do we need the RGB imagery at all? Could we achieve the same results by simply using MLST with its existing bank of functions to learn to augment our existing IR datasets? In this section we will answer these questions experimentally by learning a MLST policy for stylization, and one for augmentation. How each

model was trained is illustrated in Fig. 6. We then trained three YOLO models following the experimental design in Sec. VII with different MLST policies: one model with just an augmentation policy, one with just a stylization policy, and one using both the augmentation and stylization policies.

The results of our experiment are shown in Table IV. Both augmentation and stylization policies yield better performance for a task model on all benchmark datasets. However, MLST for stylization yields a substantially larger mAP score improvement on our detection task than MLST for augmentation. This suggests that the benefits of MLST are primarily due to effective stylization of the RGB imagery. Additionally, stylization and augmentation are additively beneficial, the model trained with both policies has an even higher mAP score.

We have observed that the stylization and augmentation policies lead to different results in Table IV. We want to consider if the training objectives of stylization and augmentation change how MLST learns to utilize the function dictionary. Do the two policies use significantly different functions? This would suggest the policies are performing distinct operations.

To aid in the understanding of policies learned by our model, it is helpful to compute two summary statistics: the expected number of times each operation is applied to an image:

$$\mathbb{E}[T^{(n)}] = \sum_k \sigma(w_k)^{(n)} \quad (9)$$

and the expected parameter value of an operation:

$$\mathbb{E}[\mu^{(n)}] = \sum_k \sigma(w_k)^{(n)} \mu_k^{(n)} \quad (10)$$

A summary of the different policies learned is shown in Fig. 7, we also include the unsupervised MLST stylization policy from Sec. VII to see if the lack of supervision significantly alters what functions MLST learns to use. We compare three policies: MLST, MSLT for augmentation, and unsupervised MLST. The results indicate that the stylization and augmentation policies are largely distinct; each policy employs the available operations at very different frequencies. The stylization uses a more diverse set of functions compared to the augmentation policy.

A. Visualization

We have shown that MLST learns a stylization that is both powerful, while not destroying the content of images; and that this policy is distinct from traditional augmentation. However, we wish to provide more evidence that MLST is meaningfully stylizing RGB imagery. We use UMAP [59] to look at the distributions of features of imagery directly by projecting them into a low dimension manifold. We looked at the UMAP projections of features extracted from the 5th convolutional layer of our YOLO model trained on the Kaist dataset. We defined four clusters corresponding to real RGB data, real IR data, stylized RGB data, and augmented IR data. The UMAP projections of features are shown in Fig. 8. For both datasets, we observe that there is are observable clusters of RGB and IR imagery. This is indicative of a measurable

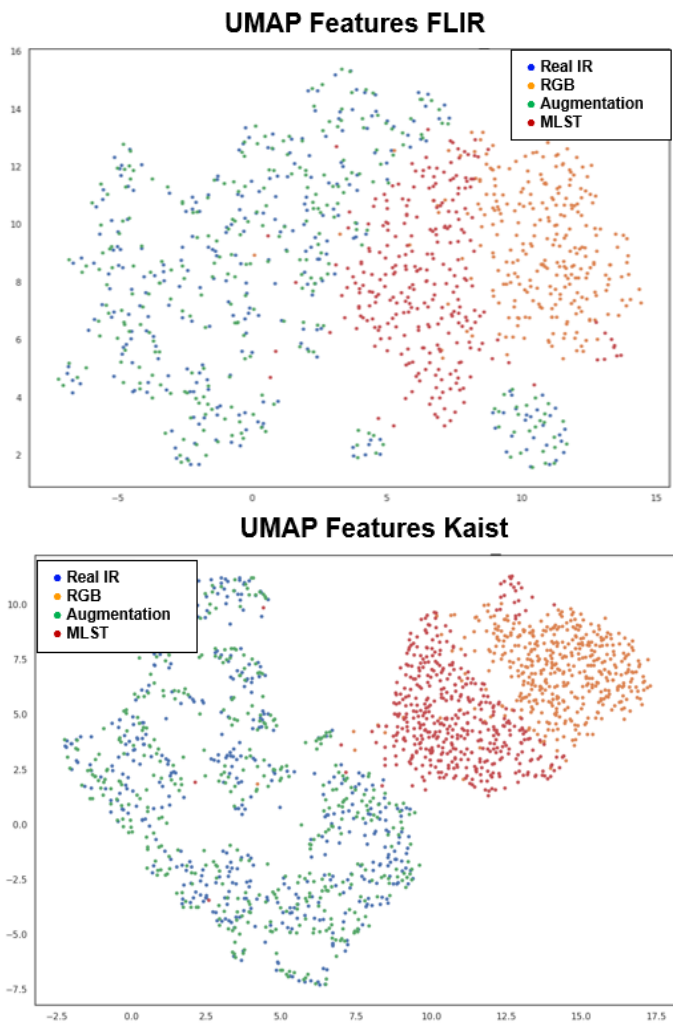


Fig. 8. This figure shows the UMAP manifolds of features extracted from a trained YOLO model on FLIR (top) and Kaist (bottom) for four classes of image: real IR (blue), RGB (orange), Augmented IR imagery (green), and MLST stylized imagery (red).

domain gap between the modalities. MLST produces a distinct cluster of imagery between the real IR and RGB images which, in addition to our experimental results in Table III, suggests MLST is closing the domain gap.

IX. SUMMARY & CONCLUSIONS

In this work we conducted experiments to measure the effectiveness of data supplementation with stylized imagery for YOLO algorithms across several IR object detection benchmark datasets. We performed controlled experiments using ten style transfer algorithms to stylize RGB images used in the training of YOLO models in conjunction with real IR data. Our experiments show that data supplementation with stylized RGB imagery yields universally higher performance on our benchmark datasets. The most effective stylization method on average was our meta-learning approach which learns a composition of functions (and function parameters) from a dictionary. We then investigated the stylizations learned by

each model and to characterize the strengths and weaknesses of each algorithm.

ACKNOWLEDGMENT

This work was supported by the U.S. Army CCDC C5ISR RTI Directorate, via a Grant Administered by the Army Research Office under Grants W911NF-06-1-0357 and W911NF-13-1-00.

REFERENCES

- [1] Y. Jing, Y. Yang, Z. Feng, J. Ye, Y. Yu, and M. Song, "Neural style transfer: A review," *IEEE transactions on visualization and computer graphics*, vol. 26, no. 11, pp. 3365–3385, 2019.
- [2] J. Deng, W. Dong, R. Socher, L.-J. Li, K. Li, and L. Fei-Fei, "Imagenet: A large-scale hierarchical image database," in *2009 IEEE conference on computer vision and pattern recognition*. Ieee, 2009, pp. 248–255.
- [3] T.-Y. Lin, M. Maire, S. Belongie, J. Hays, P. Perona, D. Ramanan, P. Dollár, and C. L. Zitnick, "Microsoft coco: Common objects in context," in *European conference on computer vision*. Springer, 2014, pp. 740–755.
- [4] E. Gebhardt and M. Wolf, "CAMEL Dataset for Visual and Thermal Infrared Multiple Object Detection and Tracking," *Proceedings of AVSS 2018 - 2018 15th IEEE International Conference on Advanced Video and Signal-Based Surveillance*, 2019.
- [5] "FLIR Thermal Datasets For Algorithm Training." [Online]. Available: <https://www.flir.com/oem/adas/adas-dataset-form/#anchor29>
- [6] C. Shorten and T. M. Khoshgoftaar, "A survey on Image Data Augmentation for Deep Learning," *Journal of Big Data*, vol. 6, no. 1, 2019. [Online]. Available: <https://doi.org/10.1186/s40537-019-0197-0>
- [7] A. Jaiswal, A. R. Babu, M. Z. Zadeh, D. Banerjee, and F. Makedon, "A Survey on Contrastive Self-Supervised Learning," *Technologies*, vol. 9, no. 1, p. 2, 2020.
- [8] K. He, "Deep Residual Learning for Image Recognition," *Proceedings of the IEEE conference on computer vision and pattern recognition*, 2016.
- [9] T. Wolf, L. Debut, V. Sanh, J. Chaumond, C. Delangue, A. Moi, P. Cistac, T. Rault, R. Louf, M. Funtowicz *et al.*, "Transformers: State-of-the-art natural language processing," in *Proceedings of the 2020 conference on empirical methods in natural language processing: system demonstrations*, 2020, pp. 38–45.
- [10] K. Weiss, T. M. Khoshgoftaar, and D. Wang, "A survey of transfer learning," *Journal of Big data*, vol. 3, no. 1, pp. 1–40, 2016.
- [11] J. Li, Q. Wang, H. Chen, J. An, and S. Li, "A Review on Neural Style Transfer," *Journal of Physics: Conference Series*, vol. 1651, no. 1, pp. 3365–3385, 2020.
- [12] C. Herrmann, M. Ruf, and J. Beyerer, "CNN-based thermal infrared person detection by domain adaptation," *Proceedings of SPIE*, vol. 1064308, no. May 2018, 2019.
- [13] J. Yoo, Y. Uh, S. Chun, B. Kang, and J.-W. Ha, "Photorealistic style transfer via wavelet transforms," in *Proceedings of the IEEE/CVF International Conference on Computer Vision*, 2019, pp. 9036–9045.
- [14] J. Hoffman, E. Tzeng, T. Park, J.-Y. Zhu, P. Isola, K. Saenko, A. Efros, and T. Darrell, "Cycada: Cycle-consistent adversarial domain adaptation," in *International conference on machine learning*. PMLR, 2018, pp. 1989–1998.
- [15] Y. Li, M.-Y. Liu, X. Li, M.-H. Yang, and J. Kautz, "A closed-form solution to photorealistic image stylization," in *Proceedings of the European Conference on Computer Vision (ECCV)*, 2018, pp. 453–468.
- [16] V. V. Kniaz, V. A. Knyaz, J. Hladuvka, W. G. Kropatsch, and V. Mizginov, "Thermalgan: Multimodal color-to-thermal image translation for person re-identification in multispectral dataset," in *Proceedings of the European Conference on Computer Vision (ECCV) Workshops*, 2018, pp. 0–0.
- [17] M. A. Özkanoğlu and S. Ozer, "Infragan: A gan architecture to transfer visible images to infrared domain," *Pattern Recognition Letters*, vol. 155, pp. 69–76, 2022.
- [18] M. Kieu, L. Berlincioni, L. Galteri, M. Bertini, A. D. Bagdanov, and A. del Bimbo, "Robust pedestrian detection in thermal imagery using synthesized images," in *2020 25th International Conference on Pattern Recognition (ICPR)*, 2021, pp. 8804–8811.
- [19] S. Liu, V. John, E. Blasch, Z. Liu, and Y. Huang, "Ir2vi: Enhanced night environmental perception by unsupervised thermal image translation," in *Proceedings of the IEEE Conference on Computer Vision and Pattern Recognition (CVPR) Workshops*, June 2018.

- [20] N. Ashikhmin, "Fast texture transfer," *IEEE computer Graphics and Applications*, vol. 23, no. 4, pp. 38–43, 2003.
- [21] H. Lee, S. Seo, S. Ryoo, and K. Yoon, "Directional texture transfer," in *Proceedings of the 8th International Symposium on Non-Photorealistic Animation and Rendering*, 2010, pp. 43–48.
- [22] L. A. Gatys, A. S. Ecker, and M. Bethge, "Image style transfer using convolutional neural networks," in *Proceedings of the IEEE conference on computer vision and pattern recognition*, 2016, pp. 2414–2423.
- [23] Y. Li, C. Fang, J. Yang, Z. Wang, X. Lu, and M.-H. Yang, "Universal style transfer via feature transforms," *Advances in neural information processing systems*, vol. 30, 2017.
- [24] Y. Li, C. Fang, J. Yang, Z. Wang, X. Lu, and M. H. Yang, "Universal style transfer via feature transforms," *Advances in Neural Information Processing Systems*, vol. 2017-December, pp. 386–396, 2017.
- [25] F. Luan, S. Paris, E. Shechtman, and K. Bala, "Deep photo style transfer," in *Proceedings of the IEEE conference on computer vision and pattern recognition*, 2017, pp. 4990–4998.
- [26] J.-Y. Zhu, T. Park, P. Isola, and A. A. Efros, "Unpaired image-to-image translation using cycle-consistent adversarial networks," in *Proceedings of the IEEE international conference on computer vision*, 2017, pp. 2223–2232.
- [27] M. S. Uddin, R. Hoque, K. A. Islam, C. Kwan, D. Gribben, and J. Li, "Converting optical videos to infrared videos using attention gan and its impact on target detection and classification performance," *Remote Sensing*, vol. 13, no. 16, p. 3257, 2021.
- [28] S. K. Jameel and J. Majidpour, "Generating spectrum images from different types—visible, thermal, and infrared based on autoencoder architecture (gvti-ae)," *International Journal of Image and Graphics*, vol. 22, no. 01, p. 2250005, 2022.
- [29] S. Cygert and A. Czyzewski, "Style transfer for detecting vehicles with thermal camera," in *2019 Signal Processing: Algorithms, Architectures, Arrangements, and Applications (SPA)*, 2019, pp. 218–222.
- [30] P. Isola, J.-Y. Zhu, T. Zhou, and A. A. Efros, "Image-to-image translation with conditional adversarial networks," in *Proceedings of the IEEE conference on computer vision and pattern recognition*, 2017, pp. 1125–1134.
- [31] R. Abbott, N. M. Robertson, J. M. del Rincon, and B. Connor, "Unsupervised object detection via lwir/rgb translation," in *Proceedings of the IEEE/CVF Conference on Computer Vision and Pattern Recognition Workshops*, 2020, pp. 90–91.
- [32] A. Buslaev, V. I. Iglovikov, E. Khvedchenya, A. Parinov, M. Druzhinin, and A. A. Kalinin, "Albumentations: Fast and Flexible Image Augmentations," *Information*, vol. 11, no. 2, pp. 1–20, 2020.
- [33] L. Li, P. Li, M. Yang, and S. Gao, "Multi-branch semantic gan for infrared image generation from optical image," in *International Conference on Intelligent Science and Big Data Engineering*. Springer, 2019, pp. 484–494.
- [34] "DSIAC ATR Algorithm Development Image Database." [Online]. Available: <https://dsiac.org/databases/atr-algorithm-development-image-database/>
- [35] Y. Choi, N. Kim, S. Hwang, K. Park, J. S. Yoon, K. An, and I. S. Kweon, "KAIST Multi-Spectral Day/Night Data Set for Autonomous and Assisted Driving," *IEEE Transactions on Intelligent Transportation Systems*, vol. 19, no. 3, pp. 934–948, 2018.
- [36] C. Devaguptapu, N. Akolekar, M. M. Sharma, and V. N. Balasubramanian, "Borrow from anywhere: Pseudo multi-modal object detection in thermal imagery," in *Proceedings of the IEEE/CVF Conference on Computer Vision and Pattern Recognition Workshops*, 2019, pp. 0–0.
- [37] R. Yadav, A. Samir, H. Rashed, S. Yogamani, and R. Dahyot, "Cnn based color and thermal image fusion for object detection in automated driving," *Irish Machine Vision and Image Processing*, 2020.
- [38] T. Hospedales, A. Antoniou, P. Micaelli, and A. Storkey, "Meta-learning in neural networks: A survey," *arXiv preprint arXiv:2004.05439*, 2020.
- [39] J. Wang, J. Xu, and X. Wang, "Combination of hyperband and bayesian optimization for hyperparameter optimization in deep learning," *arXiv preprint arXiv:1801.01596*, 2018.
- [40] Z. Li, F. Zhou, F. Chen, and H. Li, "Meta-sgd: Learning to learn quickly for few-shot learning," *arXiv preprint arXiv:1707.09835*, 2017.
- [41] M. Goldblum, L. Fowl, and T. Goldstein, "Adversarially robust few-shot learning: A meta-learning approach," *Advances in Neural Information Processing Systems*, vol. 33, pp. 17 886–17 895, 2020.
- [42] E. D. Cubuk, B. Zoph, D. Mane, V. Vasudevan, and Q. V. Le, "Autoaugmentation: Learning augmentation policies from data," *arXiv preprint arXiv:1805.09501*, 2018.
- [43] S. Lim, I. Kim, T. Kim, C. Kim, and S. Kim, "Fast autoaugment," *Advances in Neural Information Processing Systems*, vol. 32, 2019.
- [44] R. Hataya, J. Zdenek, K. Yoshizoe, and H. Nakayama, "Faster autoaugmentation: Learning augmentation strategies using backpropagation," in *European Conference on Computer Vision*. Springer, 2020, pp. 1–16.
- [45] B. Zoph, G. Ghiasi, T.-y. Lin, J. Shlens, and Q. V. Le, "Learning Data Augmentation Strategies for Object Detection," 2019.
- [46] S. Lim, I. Kim, T. Kim, C. Kim, and S. Kim, "Fast AutoAugment," *Advances in Neural Information Processing Systems*, vol. 32, 2019.
- [47] D. E. Rumelhart, G. E. Hinton, and R. J. Williams, "Learning representations by back-propagating errors," *nature*, vol. 323, no. 6088, pp. 533–536, 1986.
- [48] D. P. Kingma, T. Salimans, and M. Welling, "Variational dropout and the local reparameterization trick," *Advances in neural information processing systems*, vol. 28, 2015.
- [49] E. Jang, S. Gu, and B. Poole, "Categorical reparameterization with gumbel-softmax," *arXiv preprint arXiv:1611.01144*, 2016.
- [50] K. He, X. Zhang, S. Ren, and J. Sun, "Deep residual learning for image recognition," in *Proceedings of the IEEE conference on computer vision and pattern recognition*, 2016, pp. 770–778.
- [51] S. Li, Y. Li, Y. Li, M. Li, and X. Xu, "Yolo-firi: Improved yolov5 for infrared image object detection," *IEEE Access*, vol. 9, pp. 141 861–141 875, 2021.
- [52] R. Chen, S. Liu, J. Mu, Z. Miao, and F. Li, "Borrow from source models: Efficient infrared object detection with limited examples," *Applied Sciences*, vol. 12, no. 4, p. 1896, 2022.
- [53] H.-W. Chen, N. Gross, R. Kapadia, J. Cheah, and M. Gharbieh, "Advanced automatic target recognition (atr) with infrared (ir) sensors," in *2021 IEEE Aerospace Conference (50100)*. IEEE, 2021, pp. 1–13.
- [54] C. Kwan and J. Larkin, "Detection of small moving objects in long range infrared videos from a change detection perspective," in *Photonics*, vol. 8, no. 9. MDPI, 2021, p. 394.
- [55] P. Saha, B. A. Mudassar, and S. Mukhopadhyay, "Adaptive control of camera modality with deep neural network-based feedback for efficient object tracking," in *2018 15th IEEE International Conference on Advanced Video and Signal Based Surveillance (AVSS)*. IEEE, 2018, pp. 1–6.
- [56] X. Dai, X. Yuan, and X. Wei, "Tirnet: Object detection in thermal infrared images for autonomous driving," *Applied Intelligence*, vol. 51, no. 3, pp. 1244–1261, 2021.
- [57] G. Jocher, "Ultralytics YOLO V3." [Online]. Available: <https://github.com/ultralytics/yolov3#citation>
- [58] S. Agarwal, J. O. D. Terrail, and F. Jurie, "Recent Advances in Object Detection in the Age of Deep Convolutional Neural Networks," 2018. [Online]. Available: <http://arxiv.org/abs/1809.03193>
- [59] L. McInnes, J. Healy, and J. Melville, "UMAP: Uniform Manifold Approximation and Projection for Dimension Reduction," 2018. [Online]. Available: <http://arxiv.org/abs/1802.03426>

Evelyn A. Stump Evelyn Ann Stump was born and raised in Connecticut. She studied physics at the University of Massachusetts, Amherst where she received her B.S. in 2016. Later that year she enrolled at Duke University where she studied electrical and computer engineering under the advisement of Professors Leslie M. Collins and Jordan M. Malof and received her Ph.D. in 2022.

Francesco Luzi Francesco Luzi was born in Washington State in 1996. He studied electrical engineering at Washington State University and received his B.S. in 2017. Francesco then worked at the Pacific Northwest National Lab for several years before entering the Ph.D. program for electrical and computer engineering at Duke University in 2020 under the advisement of Dr. Leslie Collins and Dr. Jordan Malof.

Leslie M. Collins Leslie M. Collins was born in Raleigh NC. She grew up in Lexington, Kentucky and received her BSEE degree from the University of Kentucky in 1985. She received her MS degree from the EECS Department at the University of Michigan in 1986. From 1986 to 1990 she worked as a Senior Engineer at Westinghouse Research and Development in Pittsburgh, PA. She received a PhD in EECS from the University of Michigan in 1995, and subsequently joined Duke University.

Jordan M. Malof Jordan M. Malof received the B.S. degree in electrical and computer engineering from the University of Louisville, Louisville, KY, USA, in 2008, and the Ph.D. degree in electrical and computer engineering from Duke University, Durham, NC, USA, in 2015, both in electrical and computer engineering. He is currently an Assistant Professor in the Department of Computer Science at the University of Montana, where his research focuses on the development of advanced machine learning, deep learning, and computer vision to solve problems in remote sensing and scientific computing.